ROYAL SOCIETY OPEN SCIENCE

rsos.royalsocietypublishing.org

Research

Article submitted to journal

Subject Areas:
physiology, biophysics, bioengineering

Keywords:
bone, resorption, exercise

Author for correspondence:
Michael Doube
e-mail: mdoube@cityu.edu.hk

Intracortical remodelling increases in highly-loaded bone after exercise cessation

Raniere Gaia Costa da Silva[1], Tsim Christopher Sun[2], Ambika Prasad Mishra[1], Alan Boyde[3], Michael Doube[1] and Christopher Riggs[4]

[1]Department of Infectious Diseases and Public Health, City University of Hong Kong, Kowloon, Hong Kong
[2]Sydney School of Veterinary Science, University of Sydney, Camperdown, NSW, Australia
[3]Barts and The London School of Medicine and Dentistry, Queen Mary University of London, UK
[4]Department of Veterinary Clinical Services, Hong Kong Jockey Club, Hong Kong

Resorption within cortices of long bones removes excess mass and damaged tissue, and increases during periods of reduced mechanical loading. Returning to high-intensity exercise may place bones at risk of failure due to increased porosity caused by bone resorption. We used microradiographs of bone slices from highly-loaded (metacarpal, tibia, humerus) and minimally-loaded (rib) bones from 12 racehorses, 6 in high-intensity exercise and 6 that had intense exercise followed by at least 35 days of rest, and measured intracortical canal cross-sectional area (Ca.Ar) and number (N.Ca) to infer remodelling activity across sites and exercise groups. Large canals (Ca.Ar > 0.04 mm^2) were 1.4× to 18.7× greater in number and area in the third metacarpal bone from rested than exercised animals (p = 0.005–0.008), but were similar in number and area in ribs from rested and exercised animals (p = 0.575–0.688). An intermediate relationship was present in tibia and humerus, and when large canals and smaller canals (Ca.Ar > 0.002 mm^2) were considered together. The mechanostat may override targeted remodelling during periods of high mechanical load by enhancing bone formation, reducing resorption and suppressing turnover. Both systems may work synergistically in rest periods to remove excess and damaged tissue.

© 2014 The Authors. Published by the Royal Society under the terms of the Creative Commons Attribution License http://creativecommons.org/licenses/by/4.0/, which permits unrestricted use, provided the original author and source are credited.

THE ROYAL SOCIETY PUBLISHING

1. Introduction

Osteoclastic resorption of bone serves several critical functions. It is essential in the mechanism for expression of skeletal adaptation to load: resorption also facilitates the reduction of bone mass as a response to reduced loads on the skeleton [1], moulds the surfaces of bones to refine their geometric properties in response to altered strain [2–6] and is the first stage in the process to replace bone with one microstructure [7] or fibre orientation [8–12] with that of another [13]. It also facilitates the repair of bone tissue by removing damaged or dead bone matrix to make way for its replacement with healthy tissue [14–16]. Furthermore, resorption of bone is important for mineral homeostasis, providing a mechanism to release mineral ions bound in bone into circulation [17].

While osteoclastic resorption is an ongoing process in the bones of most mammals some evidence supports focal targeting of resorption in bones of the appendicular skeleton in regions where the matrix has suffered microdamage as a consequence of mechanical overload or repetitive stress injury [18,19]. Non-targeted or stochastic remodelling may occur as a homeostatic mechanism that has evolved to maintain the material health of the skeleton by reducing the effects of fatigue damage of bones in the long term [20,21]. The suppression of both targeted and stochastic remodelling by experimental administration of bisphosphonates provides support for this hypothesis [22]. Resorption, the essential first stage of the remodelling process in dense bone, creates additional porosity that may relate to higher strain energy density [2], decreased elastic modulus [23] and diminished toughness [24–26].

The loss of strength and stiffness caused by increased porosity may predispose bone to accelerated accumulation of microdamage and monotonic failure in the face of ongoing cyclical loads [20,27]. Bone must strike a balance between the risks of tissue deterioration occurring through the accumulation of microdamage with the risks of failure due to increased porosity incurred during remodelling. Previous studies indicate that the balance falls in favour of allowing microdamage to accumulate [27] rather than attempting repair by remodelling while high loads continue.

Horses are a unique model system in which to study bone dynamics. Their bones are large and support plentiful secondary osteonal remodelling [8,28–31], which does not normally occur in laboratory rodents or other mammals smaller than about 2 kg body mass [32]. Material for detailed histological study is available post-mortem from equine athletes with greater regularity and control than from human athletes. Histological examination of bone from horses used in exercise tests on treadmills [28] and from post mortem specimens from racehorses [33] suggests that osteoclastic resorption in the third metacarpal bone is suppressed in horses that are consistently subjected to a high exercise workload compared to those forced to rest. A physiological control system may have evolved to favour the safest way to manage skeletal integrity in the face of ongoing mechanical loading, but evidence for this hypothesis is weak. The purpose of the present study is to develop the evidence base to better understand bone's response to periods of intense exertion and subsequent rest.

In this study we measure bone remodelling, using the number and size of resorption canals as a proxy, in selected regions of bones from horses in active training and from horses subject to enforced rest. We use samples taken from horses for which we know the exercise history with high confidence because all the animals reside, train and race within one organisation that keeps records of all interventions.

2. Materials and Methods

(a) Study material

Bone was obtained post-mortem from Thoroughbred racehorses ($n = 12$) at the Hong Kong Jockey Club (HKJC) that had been euthanised for reasons unrelated to the study (Table 1).

Table 1. List of horses in the study.

group	ID	age (years)	intense exercise (days)	exercise-death interval (days)	cause of death
exercised	01	5	8	0	drug anaphylaxis
	02	6	8	0	tendon rupture
	03	6	6	3	collapse during racing
	04	5	4	1	colic
	05	5	6	0	collapse during racing
	06	4	6	0	collapse during fast work
	mean	5.17	6.33	0.67	
	std. dev.	0.75	1.51	1.21	
rested	07	8	5	35	advanced osteoarthritis
	08	6	5	91	tendon rupture
	09	8	5	82	chronic lameness
	10	8	4	45	advanced osteoarthritis
	11	5	5	79	unsuitable temperament
	12	6	6	94	chronic lameness
	mean	6.83	5.00	71.0	
	std. dev.	1.33	0.63	24.8	

Horses were assigned to one of two groups: "exercised" ($n = 6$) and "rested" ($n = 6$) 1. The "exercised" group was restricted to horses that had been in regular training for racing and had undertaken intense exercise within seven days of their death. "Intense exercise" was defined as a race, barrier trial (practice race), training gallop or training canter and "regular" as this level of exercise occurred on at least four occasions in the preceding 30 days. The "rested" group was restricted to horses that had previously been in race training (at which stage they had undertaken similar intense exercise to that of the "exercised" group) but that were undergoing a period of rest and had not undertaken any intense exercise for 30–120 days prior to euthanasia. Details on each horse's daily exercise were sourced from The Hong Kong Jockey Club's Racing Information database [34].

(b) Bone processing

Bone sections were cut from the right third metacarpal bone, right tibia, and left humerus, at locations that are common sites for fatigue fractures in Thoroughbred racehorses [35]. Sections were also cut from the mid-body of the tenth left rib to represent bone of the axial skeleton that is not subject to significantly altered loads during locomotion (Figure 1).

The bones were dissected in their entirety immediately post mortem. Transverse blocks of 20 mm thickness were cut from the specified region of each bone using a band saw (ST-WBS 180). The blocks from the rib, tibia and mid diaphysis of third metacarpal included the entire cross section of the bone. The blocks of the proximal humerus and distal metaphysis of the third metacarpal included only the lateral half of the entire cross section. Blocks were dissected free of soft tissue including fat and periosteum before being placed in a bacterial pronase detergent (Tergazyme 10% alkaline pronase detergent, Alconox Inc, NY, USA) at 37 °C for five days to digest remaining soft tissue. Blocks were then fixed in 70% ethanol for seven days. Plane-parallel sections 250 µm and 100 µm thick were subsequently cut from each block in a plane at right angles to the long axis of the bone using an annular saw (Leica Microsystems SP1600). Sections were stored in glycerol (Figure 2). The blocks of the distal third region of the right tibia and of the mid-diaphysis

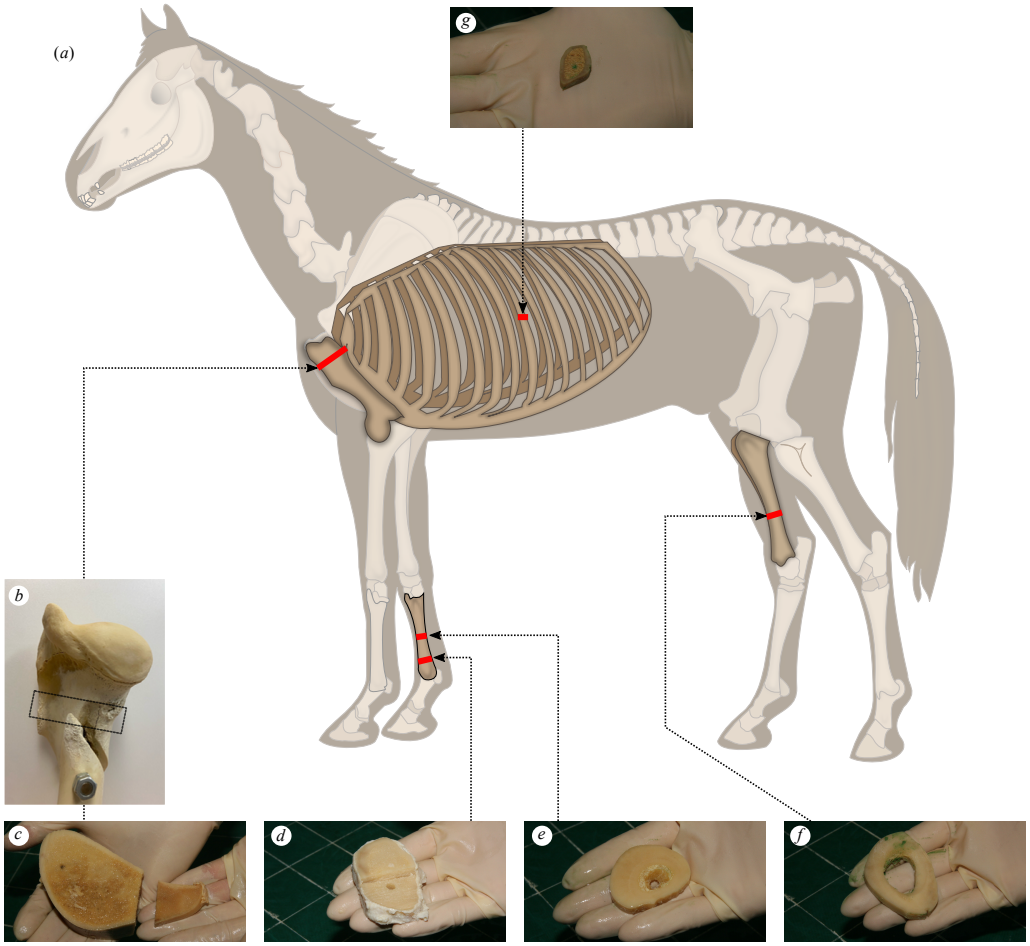

Figure 1. Sample collection sites mapped to (a) the whole horse: (b,c) proximal metaphysis of the left humerus; (d) lateral distal metaphysis of the right third metacarpal bone; (e) mid-diaphysis of the right third metacarpal bone; (f) distal third region of the right tibia; (g) mid-diaphysis of the left tenth rib. (b) Caudal view of the proximal humerus indicating the sampling site (black rectangle) and its relation to the typical location of humeral stress fracture, here demonstrated by a macerated preparation from a horse (not included in the present study) that had a complete fracture subsequent to stress fracture. This work is a derivative of "Horse anatomy.svg" by Wikipedian Prolific and Wilfredor used under Creative Commons Attribution-Share Alike 3.0 Unported licence.

of the right third metacarpal bone of horse 11 were severely damaged during cutting and could not be used.

(c) Microradiography

Microradiographs (Figure 3) were obtained from each section by point projection digital microradiography (Faxitron, QADOS, Sandhurst, Berkshire, UK) at 26 kV and the maximum magnification possible so that each section was captured in its entirety by a single image (Table 2, Figure 3). Images were stored as 8-bit TIFFs and are available from figshare (see Data Availability statement).

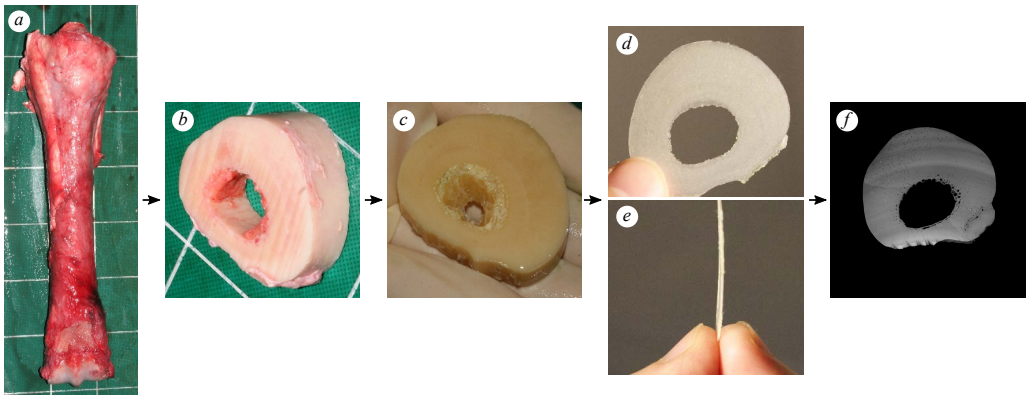

Figure 2. Bone processing from post-mortem collection to microradiograph: (a) dorsal view of the right third metacarpal bone immediately post mortem, (b) transverse 20 mm thick slice cut with a band-saw, (c) slice after five days of immersion in bacterial pronase detergent and subsequent fixation for seven days in 70% ethanol, (d) proximodistal and (e) lateral view of 250 µm thick sections cut with an annular saw, (f) microradiograph of 250 µm thick section. Dorsal to the top, medial to the right (c, d, f)

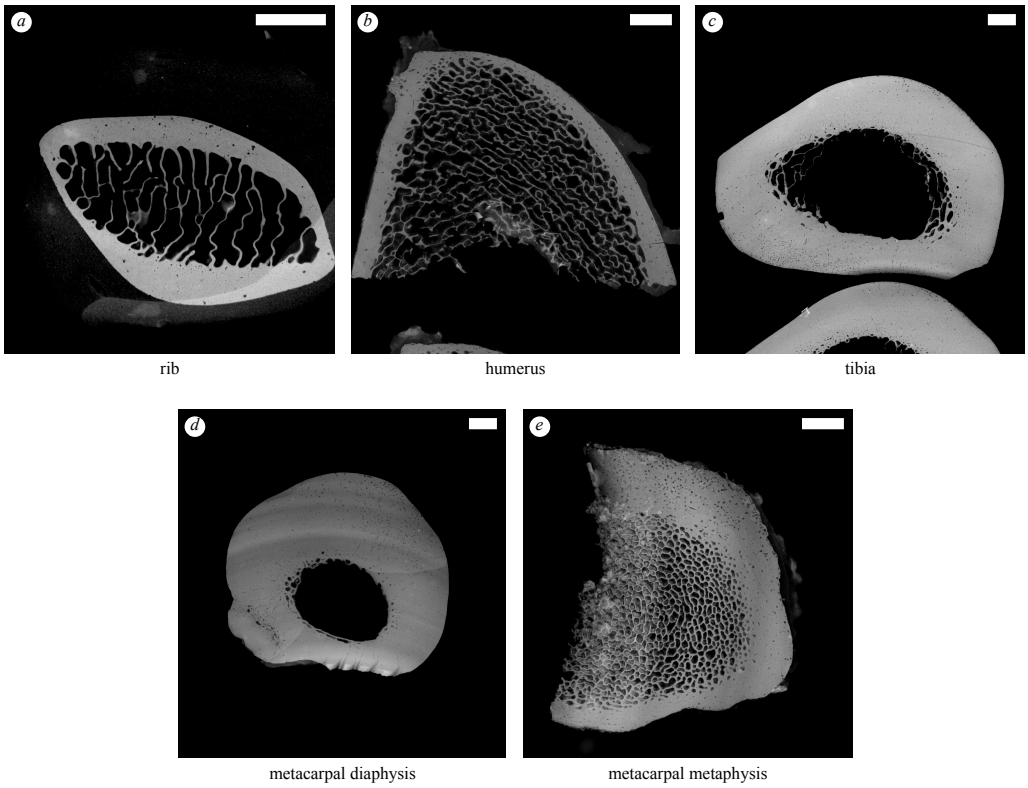

Figure 3. Example unprocessed microradiographs obtained from each section: (a) transverse section of the mid-diaphysis of the left tenth rib (5× magnification); (b) transverse section of the lateral half of the proximal left humerus (3× magnification); (c) transverse section of the distal third region of the right tibia (2× magnification); (d) transverse section of the mid-diaphysis of the right third metacarpal (2× magnification); (e) transverse section of the lateral half of the distal metaphysis of the right third metacarpal (3× magnification) (scale bars 5 mm). (a) Medial to top, cranial to left; (b) lateral to top, dorsal to right; (c) cranial to top, medial to right; (d, e) dorsal to top, medial to left.

Table 2. X-ray magnification, pixel spacing and minimum resolvable canal diameter (Ca.D) information for each sample site. The humerus from horse 5 was imaged at lower resolution than the rest of the humerus sections. Magnification was the maximum that allowed the entire specimen to be imaged in a single frame.

bone section	magnification	pixel spacing (µm)	minimum Ca.D (µm)
rib	5	10.0	11.28
humerus	3	16.7	18.84
humerus (ID 5)	2	25.0	28.21
tibia	2	25.0	28.21
metacarpal diaphysis	2	25.0	28.21
metacarpal metaphysis	3	16.7	18.84

(d) Image and Statistical Analysis

Microradiographs of each section were analysed using Fiji 1.53c [36–38] to quantify non-mineralised areas of the section (porosities) that appear as small radiolucent spots surrounded by radiopaque cortical bone matrix. Cortical bone was segmented by manually drawing along the endosteal and periosteal boundaries. A triangle method threshold [39] was calculated for each image and applied to the greyscale microradiographs, to assign each pixel to one of 'bone' or 'pore' binary phases. ImageJ's Analyze Particles function was used to identify individual pores (Figure 4c,d,e). Particles were filtered using Python to retain those with circularity between 0.3 and 1 and area > 0.002 mm^2. The smallest particles with canal area (Ca.Ar) $\leq$ 0.002 mm^2 were assumed to represent mature Haversian canals and were excluded from further analysis. Large, smooth pores at the endosteal margin of the cortex in each section that reflected transition to cancellous bone were manually excluded. Remaining pores were assumed to represent regions of bone resorption with or without subsequent formation, with the most likely descriptions corresponding to osteonal canals at the cutting cone (Ca.Ar > 0.04 mm^2) and closing cone (Ca.Ar = 0.002-0.04 mm^2) stages (Figure 4). The size categories were selected to coincide with diameters associated with mature Haversian canals (Ca.Dm, 20–30 µm in the horse) and varying stages of resorption/infilling of resorption canals [32].

The diameter of each canal (Ca.Dm, µm) was calculated from Ca.Ar assuming a circular cross section and recorded. The minimum canal diameter was slightly higher than the limit of resolution of the images (Table 2).

Cortical bone area (Ct.Ar, μm^2), count of individual canals (N.Ca, unitless), total canal area (Tt.Ca.Ar, μm^2), canal numerical density (N.Ca/Ct.Ar, μm^{-2}), and canal area fraction (Tt.Ca.Ar/Ct.Ar, unitless), were calculated for each section [41].

Differences in the measurements between exercised and rested groups were tested for using the Mann-Whitney U test, implemented in SciPy [42]. Full details of the image processing and statistical analysis are available at figshare (See Data Availability statement).

3. Results

Where groups differed, samples from the rested group contained more canals than samples from the exercised group (Figure 5, 6; Tables 3, 4, 5, 6), which was most pronounced in the metacarpal sites and for the largest canals. Numbers of canals (N.Ca/Ct.Ar) and overall porosity (Tt.Ca.Ar/Ct.Ar) were 1.4× – 18.7× greater in rested than exercised horses' metacarpal diaphysis and metacarpal metaphysis, but were not different between rested and exercised horses in the rib, humerus or tibia (Table 3, 5). A greater number of large (Ct.Ar > 0.04 mm^2) canals was evident in the dorsal cortex of the rested metacarpal diaphysis (Fig. 5i) and the caudal tibia (Fig. 5f), while a higher number of diffusely-located large canals was evident in the rested metacarpal metaphysis (Fig. 5j).

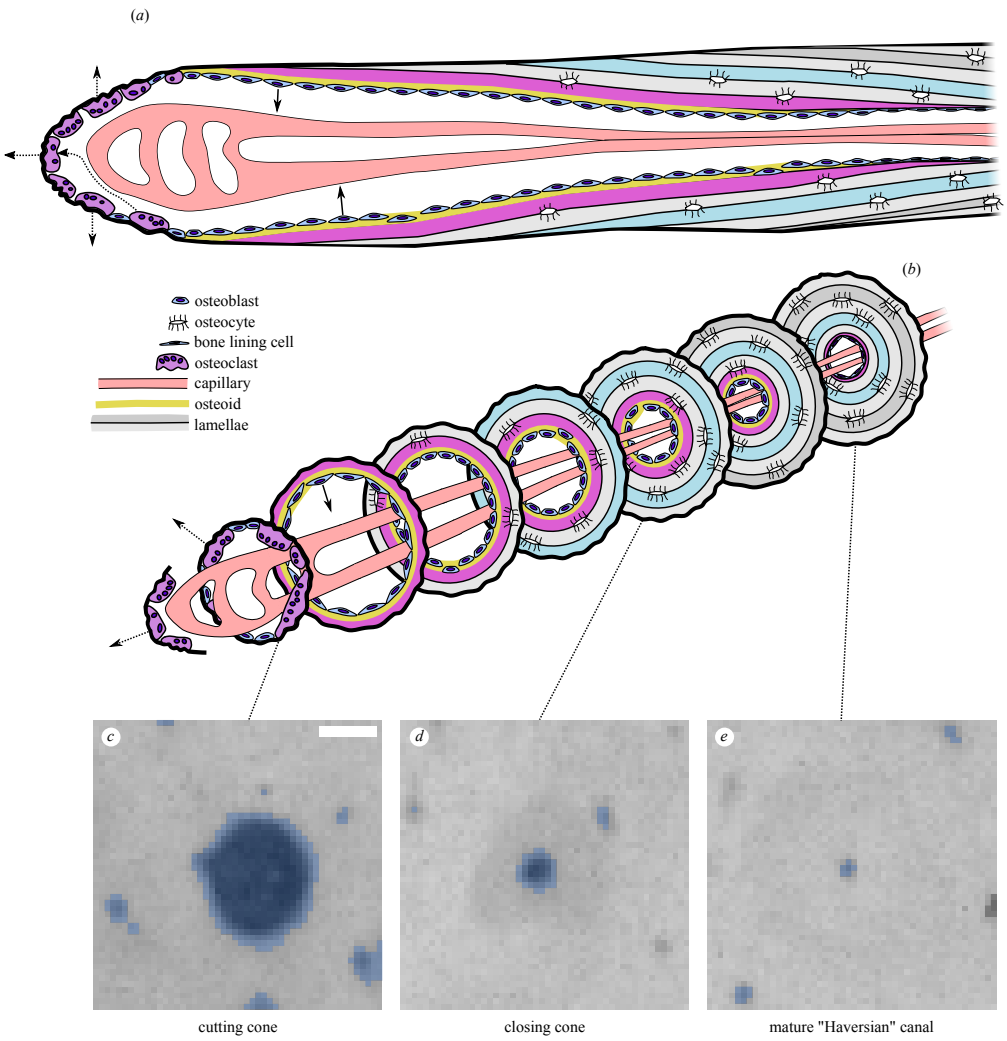

Figure 4. Illustration of secondary osteonal remodelling "basic multicellular unit" in cortical bone in (a) longitudinal section and (b) a series of transverse sections along its length. Representative microradiographs of the (c) cutting cone, (d) closing cone and (e) mature Haversian canal, shown with binary masks derived from processing with Fiji's Analyze Particles overlaid in blue. In this study we classify canals into large (Ca.Ar > 0.04 mm^2; (c)) and combined large and small (Ca.Ar > 0.002 mm^2; (c+d)), and ignore the smallest canals (Ca.Ar $\leq$ 0.002 mm^2; (e)). Scale bar 100 µm. Modified from Doube (2022) [40] under CC-BY licence terms.

Microradiographs of the humerus have considerable variation in shape and size of the bone (Figure 5c, d). Additionally, some samples presented extensive resorption in the region of the lateral cortex (Figure 7) where it was difficult to differentiate cortical bone from trabecular bone.

4. Discussion

We found significantly more and larger canals of a diameter that matches secondary osteonal remodelling events (i.e. the wide bore of cutting and closing cones) in the cortices of distal limb bones in resting horses than in horses undergoing high-intensity exercise. Assuming that the canals reflect resorptive activity, the finding provides further evidence to support the hypothesis that a physiological mechanism has evolved to limit or suppress resorption in the face of ongoing,

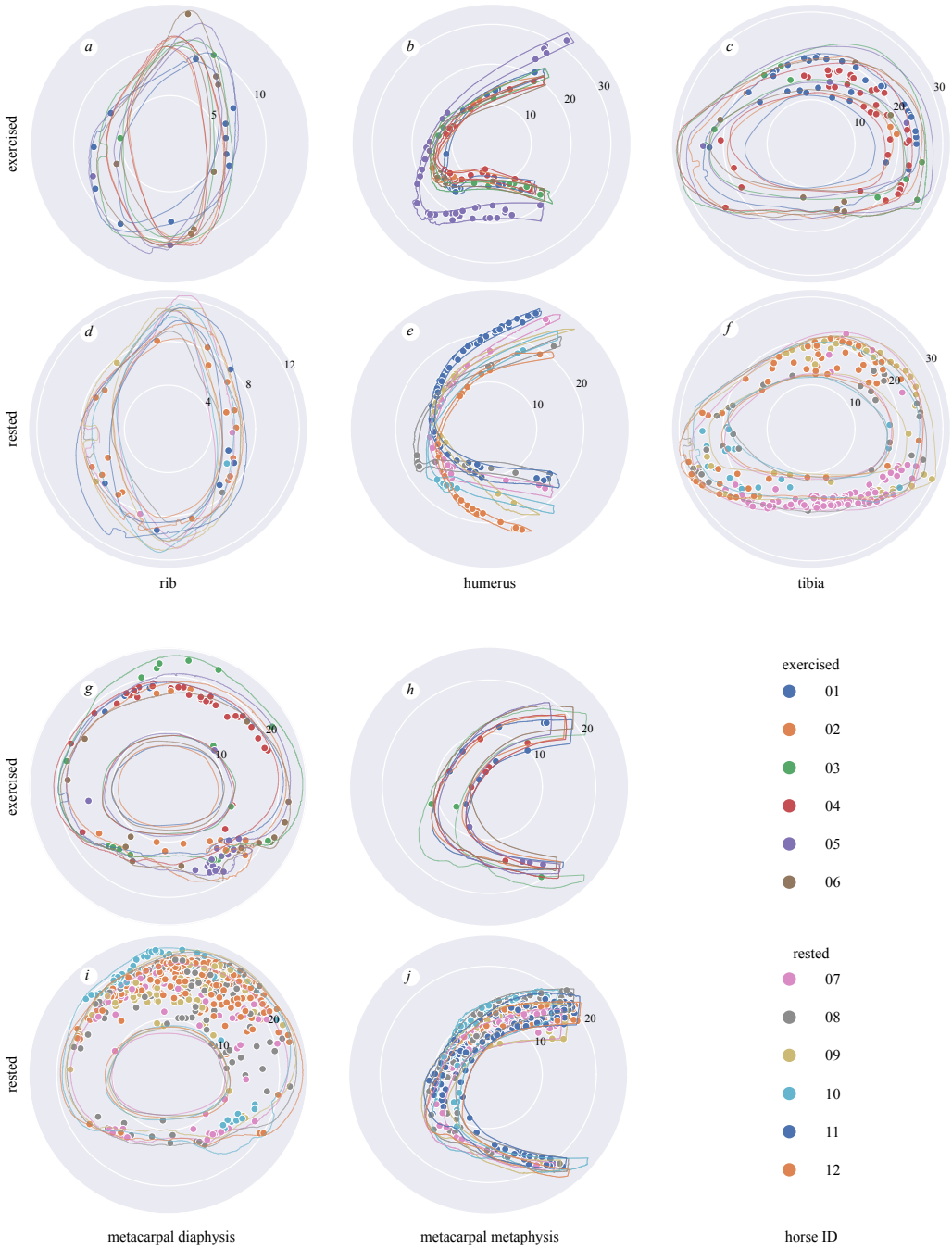

Figure 5. Polar plots of the largest canals representing resorption spaces or cutting cones (Ca.Ar > 0.04 mm^2) in bones from the exercised (a, b, c, g, h) and rested (d, e, f, i, j) groups, centred on each sample's centre of mass. Canals are indicated by solid dots, and periosteal and endosteal contours are indicated by outlines, all colour coded by horse ID. Note the larger number of large canals in the rested metacarpal and tibial sites and their anatomical distribution in the caudal tibia, dorsal metacarpal diaphysis and throughout the metacarpal metaphysis. Cranial / dorsal to the top, medial to the right. Scale in mm given by numbers indicating the radius of the white circles on each plot. See Tables 5, 6 for statistical summaries and comparisons.

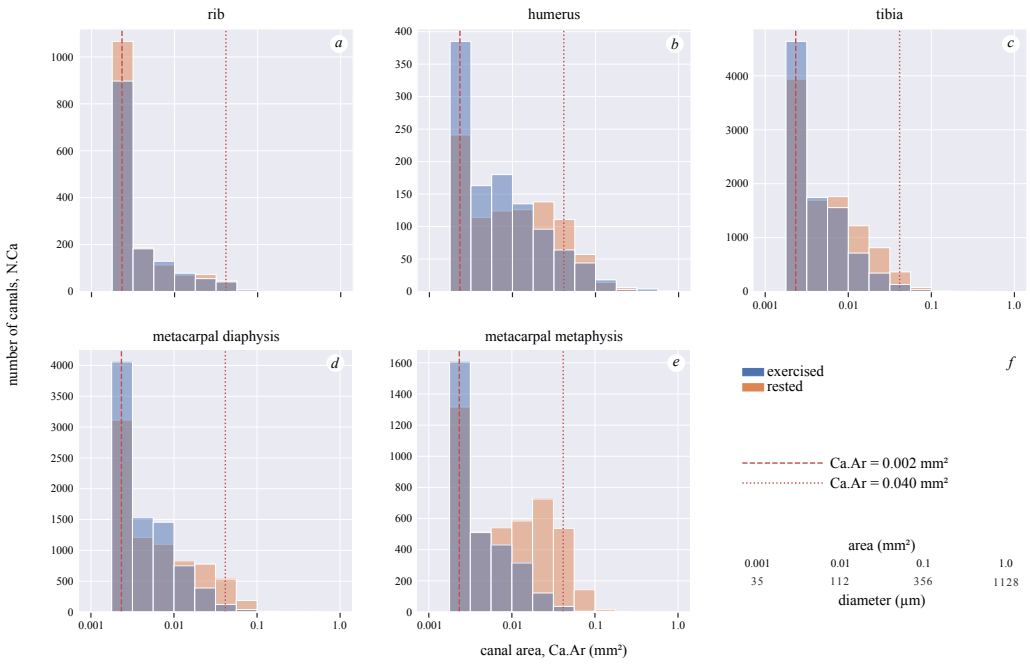

Figure 6. Canal number (N.Ca) summed over all samples within exercise and rested groups versus canal area (Ca.Ar) for canals with Ca.Ar > 0.002 mm^2, for each sample site. Note the greater number of large canals in the rested metacarpal metaphysis (e), and the similar distributions of canal sizes in rested and exercised ribs (a). See Tables 3, 4, 5, 6 for statistical summaries and comparisons. Vertical dashed line at 0.04 mm^2 indicates the cutoff value between large (resorption spaces; illustrated in Figure 5) and small (partially infilled) canals. Vertical dashed line at 0.002 mm^2 indicates the cutoff value between completely infilled mature Haversian canals and closing cones. Conversion between area and diameter assuming a circle provided in f.

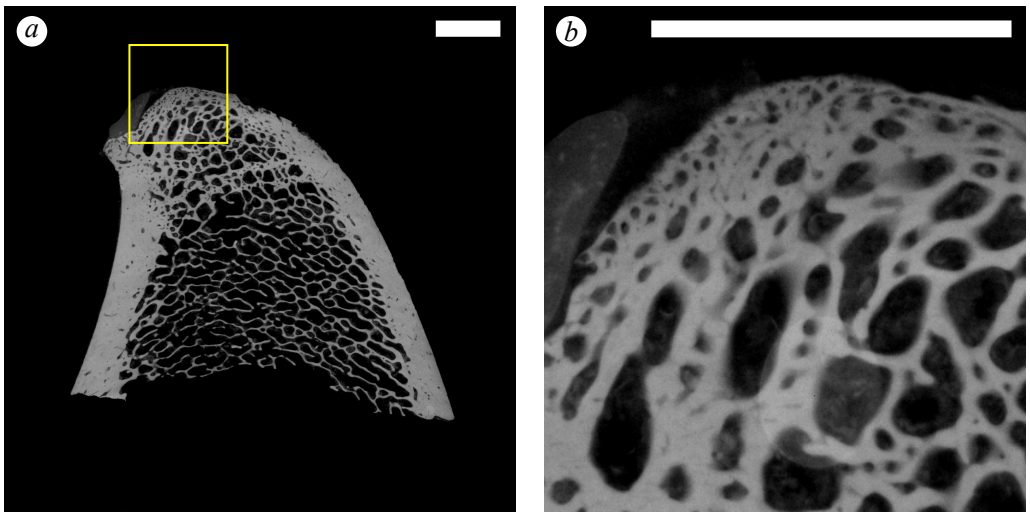

Figure 7. Illustration of lateral cortex where it was difficult to differentiate cortical bone from trabecular bone: (a) transverse section of the proximal left humerus, yellow boxed region in (a) enlarged in (b). Scale bars 5 mm.

Table 3. Summary of canal dimensions by site and exercise group (mean ± s.d.) for cutting and closing cones (Ca.Ar > 0.002 mm^2), normalised by cortical area (Ct.Ar; identical to Table 5 because they are the same specimens).

bone	group	Ct.Ar (mm^2)	N.Ca	Tt.Ca.Ar (mm^2)	N.Ca/Ct.Ar (mm^{-2})	Tt.Ca.Ar/Ct.Ar
rib	exercised	80.8 ± 5.0	232 ± 102	1.36 ± 0.97	2.82 ± 1.09	0.016 ± 0.011
	rested	79.6 ± 6.6	260 ± 130	1.49 ± 0.80	3.27 ± 1.65	0.019 ± 0.010
humerus	exercised	141 ± 49	182 ± 52	2.88 ± 1.43	1.38 ± 0.52	0.020 ± 0.006
	rested	105 ± 24	156 ± 47	3.39 ± 1.68	1.54 ± 0.61	0.033 ± 0.014
tibia	exercised	824 ± 20	1527 ± 678	9.26 ± 4.79	1.86 ± 0.82	0.011 ± 0.006
	rested	898 ± 81	1976 ± 574	17.4 ± 4.12	2.21 ± 0.67	0.019 ± 0.004
metacarpal	exercised	783 ± 73	1392 ± 561	9.06 ± 3.33	1.77 ± 0.69	0.012 ± 0.005
diaphysis	rested	816 ± 59	1552 ± 850	17.4 ± 5.80	1.92 ± 1.11	0.021 ± 0.007
metacarpal	exercised	254 ± 27	505 ± 84	3.03 ± 0.86	2.03 ± 0.49	0.012 ± 0.004
metaphysis	rested	250 ± 37	730 ± 171	11.4 ± 3.52	2.91 ± 0.58	0.046 ± 0.011

Table 4. Results of Mann-Whitney comparisons between exercised and rested groups for canals with Ca.Ar > 0.002 mm^2. *U* values tend towards 0 as the overlap between the two groups' rank distributions decreases to 0. All groups have $n = 6$ except rested tibia and rested metacarpal diaphysis which have $n = 5$.

bone	Ct.Ar		N.Ca		Tt.Ca.Ar		N.Ca/Ct.Ar		Tt.Ca.Ar/ Ct.Ar	
	U	*p*	*U*	*p*	*U*	*p*	*U*	*p*	*U*	*p*
rib	21	0.689	15	0.689	16	0.810	17	0.936	14	0.575
humerus	25	0.298	22	0.575	15	0.689	16	0.810	9	0.173
tibia	6	0.121	8	0.235	4	0.055	10	0.411	5	0.083
metacarpal diaphysis	12	0.648	16	0.927	3	0.036	16	0.927	4	0.055
metacarpal metaphysis	19	0.936	6	0.066	0	0.005	5	0.045	0	0.005

Table 5. Summary of canal dimensions by site and exercise group (mean ± s.d.) for cutting cones (Ca.Ar > 0.04 mm^2), normalised by cortical area (Ct.Ar; identical to Table 3 because they are the same specimens).

bone	group	Ct.Ar (mm^2)	N.Ca	Tt.Ca.Ar (mm^2)	N.Ca/Ct.Ar (mm^{-2})	Tt.Ca.Ar/Ct.Ar
rib	exercised	80.8 ± 5.0	3.67 ± 4.41	0.20 ± 0.25	0.04 ± 0.05	0.002 ± 0.003
	rested	79.6 ± 6.6	5.00 ± 6.63	0.26 ± 0.33	0.06 ± 0.08	0.003 ± 0.004
humerus	exercised	141 ± 49	18.2 ± 10.2	1.59 ± 1.41	0.13 ± 0.05	0.010 ± 0.005
	rested	105 ± 24	23.0 ± 17.7	1.92 ± 1.36	0.22 ± 0.15	0.018 ± 0.011
tibia	exercised	824 ± 20	165.8± 15.8	0.92 ± 0.98	0.02 ± 0.02	0.001 ± 0.001
	rested	898 ± 81	50.2 ± 26.0	2.98 ± 1.87	0.06 ± 0.03	0.003 ± 0.002
metacarpal	exercised	783 ± 73	17.0 ± 9.25	1.06 ± 0.63	0.02 ± 0.01	0.0014 ± 0.0009
diaphysis	rested	816 ± 59	93.0 ± 44.1	5.47 ± 2.49	0.11 ± 0.05	0.007 ± 0.003
metacarpal	exercised	254 ± 27	3.67 ± 3.50	0.24 ± 0.20	0.014 ± 0.014	0.0009 ± 0.0008
metaphysis	rested	250 ± 37	66.0 ± 41.6	3.89 ± 2.59	0.26 ± 0.14	0.015 ± 0.009

Table 6. Results of Mann-Whitney comparisons between exercised groups for canals with Ca.Ar > 0.04 mm^2. *U* values tend towards 0 as the overlap between the two groups' rank distributions decreases to 0. All groups have $n = 6$ except rested tibia and rested metacarpal diaphysis which have $n = 5$.

bone	Ct.Ar		N.Ca		Tt.Ca.Ar		N.Ca/Ct.Ar		Tt.Ca.Ar/ Ct.Ar	
	U	*p*	*U*	*p*	*U*	*p*	*U*	*p*	*U*	*p*
rib	21	0.689	16	0.806	15	0.688	14	0.575	15	0.688
humerus	25	0.298	17	0.936	15	0.689	12	0.378	8	0.128
tibia	6	0.121	4	0.055	5	0.083	4	0.055	5	0.083
metacarpal diaphysis	12	0.648	0	0.008	0	0.008	0	0.008	0	0.008
metacarpal metaphysis	19	0.936	0	0.005	0	0.005	0	0.005	0	0.005

high cyclical loads on bone [43,44], even while damage is accumulating. Because resorption is the first stage of intracortical remodelling, targeted remodelling of microdamaged tissue may be reduced, and not increased as suggested by others [45], while intense exercise is ongoing. Here, the rest period may have removed the suppression of resorption, allowing targeted remodelling to proceed. No relationship between osteonal remodelling and exercise group was noted in the rib, which is likely to experience only mildly elevated mechanical loads associated with increased respiratory effort at exercise.

An important function of osteoclastic resorption of bone is the repair of bone, through the replacement of damaged matrix with new, healthy tissue. Evidence that osteoclasts are recruited preferentially to target areas of microdamage or osteocyte necrosis in cortical bone [18,19,21] supports this concept. Accumulation of microdamage probably has little impact on mechanical properties of cortical bone until it becomes severe [19,21,27,46], while suppression of remodelling by half may result in 3 times the accumulation of microdamage [47,48]. In some cases, microdamage may improve the toughness of bone [49,50]. Bone repair without resorption may occur by organic and inorganic substrates bridging and sealing cracks [29,51], which might be an inherent property of mineralised tissues occurring across all vertebrate taxa like bone remodelling is [52]. In vitro mechanical testing of bone specimens machined from the third metacarpal of Thoroughbred racehorses showed that the elastic modulus and yield strength of specimens were not significantly affected by prior fatigue loading equivalent to a lifetime of racing [53]. Conversely, there is good evidence that cortical porosity is negatively correlated with Young's modulus [25], compressive ultimate stress [54], and fracture toughness [49]. Changes in porosity account for more than 75% of the variability in the strength of the cortical bone [55], and fatigue-induced microdamage located near cortical pores may be more likely to lead to fracture than that located in regions of high mineral content [56].

In the present study, resorption was determined by mapping porosities, which were assumed to represent resorption spaces, partially-infilled canals and mature Haversian canals, whose number and size may be an accurate histological measurement of bone remodelling [21,57]. Resorption spaces in cortical bone may be the classical cutting cone passing through bone matrix, or resorption occurring on the surface of existing osteonal canals [3,58]. Porosities within cortical bone are typically present in the form of osteocyte lacunae ($< 5\,\mu$m diameter) with associated, tortuous interconnected canaliculi ($< 1\,\mu$m diameter); Haversian canals at the centre of osteons (c. $20\,\mu$m diameter); Volkmann's canals, running roughly perpendicular to Haversian canals; resorption canals, in varying stages of being infilled with new bone (between 10 and $400\,\mu$m). Haversian and resorption canals are roughly circular to ellipsoidal in cross section. The former two predominantly lie parallel with the long axis of the bone and so appear circular in transverse section of long bones. Conversely Volkmann's canals appear as tubular or elongated oval structures, depending on their precise orientation relative to the plane of section. Occasionally, larger (>$600\,\mu$m wide), irregular porosities are present close to the endosteal surface of long bones, representing a transition to trabecular bone [3]. We managed these by manually excluding them during segmentation. The presence of such features was particularly common in the location studied in the proximal humerus.

Osteonal canals rapidly infill, and subperiosteal primary osteonal bone growth may occur early in training [28], conforming to the mechanostat model whereby increased strains lead to net bone deposition [59]. Our data broadly agree with the mechanostat in that the bone regions that experienced the most intense difference in loads (metacarpal diaphysis) responded the most markedly in terms of osteonal infilling (small canals) under exercise and bone resorption (large canals) during rest. Some resorption, indicated by a small number of large canals, may occur even in the most highly-loaded regions (Figure 6), consistent with previous findings [33].

Complete fracture of bones of the appendicular skeleton as a consequence of extension of stress fractures is relatively common in racehorses and represents a serious threat to horse welfare [60–63]. Better understanding of the natural biology of bone, especially in relation to repair of microdamage and how the mechanical integrity of the bone may be undermined by the repair

process, is necessary in order to develop management strategies to mitigate risk. The high number of large canals observed in the rested group has important implications for physical activity management [64–67], in particular the re-introduction of training after returning from a prolonged rest period. High porosity may be related to reduced bone yield stress and stiffness [25,68,69] and may also create stress risers allowing fracture propagation [70]. Physical readiness training, reduced marching, exercise on flat rather than hilly terrain, and adhering to an exercise protocol, reduces stress fractures of the lower limb bones in human military recruits [71,72].

There is epidemiological evidence that racehorses returning after an eight week rest period are at greater risk of sustaining complete fractures of the humerus, scapula and tibia [61–63]. It remains to be seen whether a gradual programme of exercise reintroduction is more bone-safe, and this study did not detect a strong bone remodelling signal in the humeral site examined. The time taken for completion of bone remodelling is unknown, however, osteoclasts proceed longitudinally through bone at a rate of about 40 µm d^{-1} [73], while osteoblastic infilling starts at the same time radial resorption ends [74] and at 1.0–1.5 µm d^{-1} [28,75] should take 60–90 days to infill from cement line (c. 100 µm radius) to finished canal (c. 10 µm radius) [32]. Completion of remodelling at the organ scale relies on a number of secondary osteons working asynchronously in different locations and is likely to be complicated by individual variations in bone loading, training and resting patterns. Gentle preconditioning exercise that stimulates infilling and that does not suppress targeted remodelling is desirable, but the specific training regimens required to achieve this remain obscure.

Healed fractures are very common among mammals having appeared early in vertebrate evolution [52], suggesting a survival advantage to risking fracture events because fractured bones have the capacity to heal well. We speculate that it may be a lesser cost to the organism to accumulate microdamage and defer remodelling during chronic high load periods, than to incur both high metabolic cost and increased fracture risk by resorbing highly-loaded bone.

While the most plausible biological explanation for the increased number and size of canals is associated with the remodelling process that occurs with low levels of mechanical loading, the association between duration of rest period and age is unknown. We selected a rest period of 4–16 weeks based on results of previous studies [76–78] in which bone resorption was detected between 4 and 16 weeks.

To the authors' knowledge, no previous studies have reported on the differences in fracture-free bone resorption between exercised and rested racehorses. Choosing non-fractured horses was paramount as horses with diagnosed catastrophic or non-catastrophic fractures may have had altered normal bone loading patterns and would not be truly representative of bone loading and resorption, although it was possible that other non-fracture related reasons may also have caused significant lameness that may have reduced the intensity of bone loading during high intensity exercise. Furthermore, this selection criterion resulted in a small sample size of 12 horses, which limits the power of the study to detect small differences between groups and increased the possibility of random error. Matching for age was not considered practical and would have further reduced case numbers; failure to do so here resulted in the exercised horses being on average younger than the rested horses (Table 1) [79]. We considered that restricting the selection criterion to high intensity exercise was appropriate because it has the advantage of reducing the confounding influence of training variation between horses, and is consistent with the design of other studies in the field [33,79,80]. The loss of a tibia specimen was unfortunate because the two- to three-fold difference in N.Ca/Ct.Ar and Tt.Ca.Ar/Ct.Ar for cutting cone-sized canals in the tibial site cannot be considered a robust result and is merely suggestive.

It was not possible to cut 100 µm sections from the entire cross section of the proximal humerus or the distal metaphysis of the third metacarpal bone and so our analysis was restricted to the lateral half of each bone in these locations. Consequently, the area of cortical bone studied from the proximal humerus did not precisely match that where stress fractures arise as it included only part of the caudal cortex (the usual focus of pathology) and the deltoid crest and, in some cases, part of the deltoid tuberosity. It is possible that we underestimated the extent of resorption

in cortical bone in the proximal humerus for this reason [81]. Further, our results may have been confounded by the effects of insertion of the deltoid muscle on local bone mechanics in this region. The palmarolateral cortex of the third metacarpal bone is the most common location for stress fractures in the distal metaphyseal region of this bone [82] and, therefore, we believe that the results from this location are more likely to reflect relevant findings. The anatomical location from which specimens from the tibia were sampled was chosen because this is a common location for stress fractures to occur in our population of horses based on diagnosis by nuclear scintigraphy. While others have reported the same finding in other jurisdictions [83], it is noteworthy that complete fracture of the tibia due to stress fracture is much more common in the proximal tibia [62]. Consequently, intra-cortical resorption may be much more intense in bone of the proximal tibia than we determined from this study and this limitation should be borne in mind when interpreting our results.

The numerical cutoffs that we used to classify canals into large and small groups are a simplification that aids in interpretation. The microradiographic data presented here do not capture the physiological status of each canal, only their sizes. We are also aware that a hard cutoff does not necessarily represent the diversity of modes by which resorption and infilling may occur and their dynamic nature, including substantial resting periods where neither resorption nor deposition are occurring. We believe that it is helpful to separate the very largest canals (Ca.Ar > 0.04 mm^2; resorption space, cutting cone) from the moderately-sized (Ca.Ar > 0.002 mm^2; infilling canal, closing cone) and smallest canals (Ca.Ar < 0.002 mm^2; mature, Haversian canal) because these categories give some insight into the overall status of the bone and in particular whether porosity that can have resulted only from resorption is more or less common depending on the exercise or rested status of the animal.

Variation in bone geometry was minimised by cutting bone blocks in pre-determined standardised locations and visualising canals relative to the bone section's centre of mass (Figure 5). The relationship between bone remodelling and bone geometry was not within the scope of this study but is likely to be affected by differences in mechanical loading [84–86], and changes to the second moment of area [87,88] to minimise peak bone strains. It is therefore not unreasonable to assume that different training regimens may have influenced the geometry of some of the bone sections, and the relationship between bone resorption and bone geometry should be explored in future studies. The counting of canals was automated with Fiji [36–38] which should have reduced bias. A thresholding technique was used for porosity segmentation but did contend with substantial variation in background intensity due to uneven sample thickness. Given the aim of this study, two-dimensional microradiography was considered a suitable imaging technique to identify bone resorption, however, future studies should use three dimensional imaging techniques such as X-ray microtomography and incorporate other markers of bone remodelling such as intra-vital calcein labelling to evaluate bone formation rate [75].

5. Conclusion

We found in distal limb bones, but not in ribs, that total canal area and the number of large canals, representing resorption activity, were greater in rested than in exercised animals, and that large canals were concentrated in regions known to experience high strains during peak athletic loading. We surmise that the resorption phase of bone remodelling is significantly suppressed by high intensity exercise and is subsequently reactivated during a rest period to repair accumulated microdamage in a site-specific manner. During high intensity exercise periods, the balance between the mechanostat (increasing bone mass) and targeted remodelling (increased secondary osteonal cutting cone formation) appears to tilt towards the mechanostat. Targeted remodelling and the mechanostat may work synergistically in rest periods to remove damaged and excess bone tissue. Numerous large canals might exacerbate the risk of catastrophic failure should intense exercise be reintroduced prior to osteoblastic infilling that completes the bone remodelling cycle. Future studies should be directed at determining appropriate training regimens to protect athletes' bones when they return to exercise following an extended period of rest.

6. Ethical Statement

Post-mortem material was derived from racehorses that died for reasons unrelated to the current study. Permission to use residual tissues is granted by the Hong Kong Jockey Club ownership agreement. Racing and training information was taken from publicly available data.

7. Data accessibility

All raw images are available at doi:10.6084/m9.figshare.c.5910674. Bone statistics from the raw images are available at doi:10.6084/m9.figshare.19410431. Pore information from the raw images is available at doi:10.6084/m9.figshare.19410452. Full details of the image processing and statistical analysis are available at doi:10.6084/m9.figshare.19418933.

8. Authors' contributions

Raniere Gaia Costa da Silva: formal analysis, methodology, writing original draft, review and editing. Tsim Christopher Sun: methodology, writing original draft, review and editing. Ambika Prasad Mishra: writing review. Alan Boyde: methodology. Michael Doube: supervision, writing original draft, writing review and editing. Christopher Riggs: supervision, conceptualization, methodology, writing original draft, writing review and editing. All authors gave final approval for publication and agreed to be held accountable for the work performed therein.

9. Competing interests

At the time this manuscript was considered and accepted for publication Michael Doube was a member of the Editorial Board for Royal Society Open Science but had no involvement in the assessment of the manuscript.

10. Funding

RGCdS was supported by a City University of Hong Kong Postgraduate Studentship funded by a Hong Kong University Grants Committee-related research project (9610446).

11. Acknowledgements

We thank the two reviewers for their comments that helped us to improve the presentation of this work.

References

1. Lang T, LeBlanc A, Evans H, Lu Y, Genant H, Yu A. 2004 Cortical and Trabecular Bone Mineral Loss From the Spine and Hip in Long-Duration Spaceflight. *Journal of Bone and Mineral Research* **19**, 1006–1012.
2. Bakalova LP, Andreasen CM, Thomsen JS, Brüel A, Hauge EM, Kiil BJ, Delaisse JM, Andersen TL, Kersh ME. 2018 Intracortical Bone Mechanics Are Related to Pore Morphology and Remodeling in Human Bone. *Journal of Bone and Mineral Research: The Official Journal of the American Society for Bone and Mineral Research* **33**, 2177–2185.
3. Andreasen CM, Bakalova LP, Brüel A, Hauge EM, Kiil BJ, Delaisse JM, Kersh ME, Thomsen JS, Andersen TL. 2020 The generation of enlarged eroded pores upon existing intracortical canals is a major contributor to endocortical trabecularization. *Bone* **130**, 115127.
4. Shaw CN, Ryan TM. 2012 Does skeletal anatomy reflect adaptation to locomotor patterns? cortical and trabecular architecture in human and nonhuman anthropoids. *American Journal of Physical Anthropology* **147**, 187–200.

5. Shaw CN, Stock JT. 2009 Intensity, repetitiveness, and directionality of habitual adolescent mobility patterns influence the tibial diaphysis morphology of athletes. *American Journal of Physical Anthropology* **140**, 149–159.
6. Ireland A, Maden-Wilkinson T, Ganse B, Degens H, Rittweger J. 2014 Effects of age and starting age upon side asymmetry in the arms of veteran tennis players: a cross-sectional study. *Osteoporosis International* **25**, 1389–1400.
7. Busse B, Hahn M, Schinke T, Püschel K, Duda GN, Amling M. 2010 Reorganization of the femoral cortex due to age-, sex-, and endoprosthetic-related effects emphasized by osteonal dimensions and remodeling. *Journal of Biomedical Materials Research Part A* **92A**, 1440–1451.
8. Riggs CM, Lanyon LE, Boyde A. 1993a Functional associations between collagen fibre orientation and locomotor strain direction in cortical bone of the equine radius. *Anatomy and Embryology* **187**, 231–8.
9. Riggs CM, Vaughan LC, Evans GP, Lanyon LE, Boyde A. 1993b Mechanical implications of collagen fibre orientation in cortical bone of the equine radius. *Anatomy and Embryology* **187**, 239–248.
10. McFarlin SC, Terranova CJ, Zihlman AL, Enlow DH, Bromage TG. 2008 Regional variability in secondary remodeling within long bone cortices of catarrhine primates: the influence of bone growth history. *Journal of Anatomy* **213**, 308–324.
11. Goldman HM, Hampson NA, Guth JJ, Lin D, Jepsen KJ. 2014 Intracortical Remodeling Parameters Are Associated With Measures of Bone Robustness. *The Anatomical Record* **297**, 1817–1828.
12. Goldman HM, Bromage TG, Thomas CDL, Clement JG. 2003 Preferred collagen fiber orientation in the human mid-shaft femur. *The Anatomical Record* **272A**, 434–445.
13. Collins CJ, Kozyrev M, Frank M, Andriotis OG, Byrne RA, Kiener HP, Pretterklieber ML, Thurner PJ. 2019 The impact of age, mineralization, and collagen orientation on the mechanics of individual osteons from human femurs. *Materialia* p. 100573.
14. Mori S, Burr DB. 1993 Increased intracortical remodeling following fatigue damage. *Bone* **14**, 103–109.
15. Burr DB, Martin RB, Schaffler MB, Radin EL. 1985 Bone remodeling in response to in vivo fatigue microdamage. *Journal of Biomechanics* **18**, 189–200.
16. Lee TC, Staines A, Taylor D. 2002 Bone adaptation to load: microdamage as a stimulus for bone remodelling. *Journal of Anatomy* **201**, 437–446.
17. Cappariello A, Maurizi A, Veeriah V, Teti A. 2014 The Great Beauty of the osteoclast. *Archives of Biochemistry and Biophysics* **558**, 70–78.
18. Martin RB. 2007 Targeted bone remodeling involves BMU steering as well as activation. *Bone* **40**, 1574–1580.
19. Plotkin LI. 2014 Apoptotic osteocytes and the control of targeted bone resorption. *Current osteoporosis reports* **12**, 121–126.
20. Frank JD, Ryan M, Kalscheur VL, Ruaux-Mason CP, Hozak RR, Muir P. 2002 Aging and accumulation of microdamage in canine bone. *Bone* **30**, 201–206.
21. Parfitt A. 2002 Targeted and nontargeted bone remodeling: relationship to basic multicellular unit origination and progression. *Bone* **30**, 5–7.
22. Li J, Mashiba T, Burr D. 2001 Bisphosphonate Treatment Suppresses Not Only Stochastic Remodeling but Also the Targeted Repair of Microdamage. *Calcified Tissue International* **69**, 281–286.
23. Gibson VA, Stover SM, Gibeling JC, Hazelwood SJ, Martin RB. 2006 Osteonal effects on elastic modulus and fatigue life in equine bone. *Journal of Biomechanics* **39**, 217–225.
24. Bell KL, Loveridge N, Power J, Garrahan N, Meggitt BF, Reeve J. 1999 Regional differences in cortical porosity in the fractured femoral neck. *Bone* **24**, 57–64.
25. Schaffler MB, Burr DB. 1988 Stiffness of compact bone: Effects of porosity and density. *Journal of Biomechanics* **21**, 13–16.
26. Yeni YN, Brown CU, Wang Z, Norman TL. 1997 The influence of bone morphology on fracture toughness of the human femur and tibia. *Bone* **21**, 453–459.
27. Seref-Ferlengez Z, Kennedy OD, Schaffler MB. 2015 Bone microdamage, remodeling and bone fragility: how much damage is too much damage?. *BoneKEy Reports* **4**, 644.
28. Firth EC, Rogers CW, Doube M, Jopson NB. 2005 Musculoskeletal responses of 2-year-old Thoroughbred horses to early training. 6. Bone parameters in the third metacarpal and third metatarsal bones. *New Zealand Veterinary Journal* **53**, 101–112.

29. Boyde A. 2003 The real response of bone to exercise. *Journal of Anatomy* **203**, 173–189. PMC1571152.
30. Stover SM, Pool RR, Martin RB, Morgan JP. 1992 Histological features of the dorsal cortex of the third metacarpal bone mid-diaphysis during postnatal growth in thoroughbred horses. *Journal of Anatomy* **181 (Pt 3)**, 455–469.
31. Shahar R, Lukas C, Papo S, Dunlop JW, Weinkamer R. 2011 Characterization of the Spatial Arrangement of Secondary Osteons in the Diaphysis of Equine and Canine Long Bones. *The Anatomical Record: Advances in Integrative Anatomy and Evolutionary Biology* **294**, 1093–1102.
32. Felder AA, Phillips C, Cornish H, Cooke M, Hutchinson JR, Doube M. 2017 Secondary osteons scale allometrically in mammalian humerus and femur. *Royal Society Open Science* **4**, 170431.
33. Whitton RC, Mirams M, Mackie EJ, Anderson GA, Seeman E. 2013 Exercise-induced inhibition of remodelling is focally offset with fatigue fracture in racehorses. *Osteoporosis International* **24**, 2043–2048.
34. The Hong Kong Jockey Club. 2021 Racing Information Database. .
35. Riggs CM, Pilsworth R. 2014 Repetitive strain injuries of the skeleton in high performance equine athletes. In Hinchcliff KW, Kaneps AJ, Geor RJ, editors, *Equine Sports Medicine and Surgery* , pp. 457–471. W.B. Saunders second edition edition.
36. Schindelin J, Arganda-Carreras I, Frise E, Kaynig V, Longair M, Pietzsch T, Preibisch S, Rueden C, Saalfeld S, Schmid B, Tinevez JY, White DJ, Hartenstein V, Eliceiri K, Tomancak P, Cardona A. 2012 Fiji: an open-source platform for biological-image analysis. *Nature Methods* **9**, 676–682.
37. Rueden CT, Schindelin J, Hiner MC, DeZonia BE, Walter AE, Arena ET, Eliceiri KW. 2017 ImageJ2: ImageJ for the next generation of scientific image data. *BMC bioinformatics* **18**, 529.
38. Schneider CA, Rasband WS, Eliceiri KW. 2012 NIH Image to ImageJ: 25 years of image analysis. *Nature Methods* **9**, 671–675.
39. Zack GW, Rogers WE, Latt SA. 1977 Automatic measurement of sister chromatid exchange frequency.. *Journal of Histochemistry & Cytochemistry* **25**, 741–753. Publisher: Journal of Histochemistry & Cytochemistry.
40. Doube M. 2022 Closing cones create conical lamellae in secondary osteonal bone. *Royal Society Open Science* **9**, 220712.
41. Dempster DW, Compston JE, Drezner MK, Glorieux FH, Kanis JA, Malluche H, Meunier PJ, Ott SM, Recker RR, Parfitt AM. 2013 Standardized Nomenclature, Symbols, and Units for Bone Histomorphometry: A 2012 Update of the Report of the ASBMR Histomorphometry Nomenclature Committee. *Journal of bone and mineral research : the official journal of the American Society for Bone and Mineral Research* **28**, 2–17.
42. SciPy 1.0 Contributors, Virtanen P, Gommers R, Oliphant TE, Haberland M, Reddy T, Cournapeau D, Burovski E, Peterson P, Weckesser W, Bright J, van der Walt SJ, Brett M, Wilson J, Millman KJ, Mayorov N, Nelson ARJ, Jones E, Kern R, Larson E, Carey CJ, Polat , Feng Y, Moore EW, VanderPlas J, Laxalde D, Perktold J, Cimrman R, Henriksen I, Quintero EA, Harris CR, Archibald AM, Ribeiro AH, Pedregosa F, van Mulbregt P. 2020 SciPy 1.0: fundamental algorithms for scientific computing in Python. *Nature Methods* **17**, 261–272.
43. Komori T. 2013 Functions of the osteocyte network in the regulation of bone mass. *Cell and Tissue Research* **352**, 191–198.
44. Dittmer KE, Firth EC. 2017 Mechanisms of bone response to injury. *Journal of Veterinary Diagnostic Investigation* **29**, 385–395. Publisher: SAGE Publications Inc.
45. Hughes JM, Castellani CM, Popp KL, Guerriere KI, Matheny RW, Nindl BC, Bouxsein ML. 2020 The Central Role of Osteocytes in the Four Adaptive Pathways of Bone's Mechanostat. *Exercise and Sport Sciences Reviews* **48**, 140–148.
46. Norman TL, Yeni YN, Brown CU, Wang Z. 1998 Influence of microdamage on fracture toughness of the human femur and tibia. *Bone* **23**, 303–306.
47. Allen MR, Iwata K, Phipps R, Burr DB. 2006 Alterations in canine vertebral bone turnover, microdamage accumulation, and biomechanical properties following 1-year treatment with clinical treatment doses of risedronate or alendronate. *Bone* **39**, 872–879.
48. Mashiba T, Hirano T, Turner CH, Forwood MR, Johnston CC, Burr DB. 2000 Suppressed bone turnover by bisphosphonates increases microdamage accumulation and reduces some biomechanical properties in dog rib. *Journal of Bone and Mineral Research: The Official Journal of the American Society for Bone and Mineral Research* **15**, 613–620.
49. Ural A, Vashishth D. 2007 Effects of intracortical porosity on fracture toughness in aging human bone: a microCT-based cohesive finite element study. *Journal of Biomechanical Engineering* **129**, 625–631.

50. Nalla RK, Stölken JS, Kinney JH, Ritchie RO. 2005 Fracture in human cortical bone: local fracture criteria and toughening mechanisms. *Journal of Biomechanics* **38**, 1517–1525.
51. Seref-Ferlengez Z, Basta-Pljakic J, Kennedy OD, Philemon CJ, Schaffler MB. 2014 Structural and mechanical repair of diffuse damage in cortical bone in vivo. *Journal of Bone and Mineral Research* **29**, 2537–2544.
52. Herbst EC, Doube M, Smithson TR, Clack JA, Hutchinson JR. 2019 Bony lesions in early tetrapods and the evolution of mineralized tissue repair. *Paleobiology* **45**, 676–697.
53. Martin RB, Stover SM, Gibson VA, Gibeling JC, Griffin LV. 1996 In vitro fatigue behavior of the equine third metacarpus: remodeling and microcrack damage analysis. *Journal of Orthopaedic Research: Official Publication of the Orthopaedic Research Society* **14**, 794–801.
54. Behrens JC, Walker PS, Shoji H. 1974 Variations in strength and structure of cancellous bone at the knee. *Journal of Biomechanics* **7**, 201–207.
55. McCalden RW, McGeough JA, Barker MB, Court-Brown CM. 1993 Age-related changes in the tensile properties of cortical bone. The relative importance of changes in porosity, mineralization, and microstructure. *The Journal of Bone and Joint Surgery. American Volume* **75**, 1193–1205.
56. Turnbull TL, Baumann AP, Roeder RK. 2014 Fatigue microcracks that initiate fracture are located near elevated intracortical porosity but not elevated mineralization. *Journal of Biomechanics* **47**, 3135–3142.
57. Frost HM. 1969 Tetracycline-based histological analysis of bone remodeling. *Calcified Tissue Research* **3**, 211–237.
58. Andreasen CM, Delaisse JM, van der Eerden BC, van Leeuwen JP, Ding M, Andersen TL. 2018 Understanding Age-Induced Cortical Porosity in Women: The Accumulation and Coalescence of Eroded Cavities Upon Existing Intracortical Canals Is the Main Contributor. *Journal of Bone and Mineral Research* **33**, 606–620. _eprint: https://asbmr.onlinelibrary.wiley.com/doi/pdf/10.1002/jbmr.3354.
59. Frost HM. 2003 Bone's mechanostat: A 2003 update. *Anatomical Record* **275A**, 1081–1101.
60. Riggs CM, Whitehouse GH, Boyde A. 1999 Pathology of the distal condyles of the third metacarpal and third metatarsal bones of the horse. *Equine Veterinary Journal* **31**, 140–148.
61. Vallance SA, Entwistle RC, Hitchens PL, Gardner IA, Stover SM. 2013 Case-control study of high-speed exercise history of Thoroughbred and Quarter Horse racehorses that died related to a complete scapular fracture: Exercise history of racehorses with a catastrophic scapular fracture. *Equine Veterinary Journal* **45**, 284–292.
62. Samol MA, Uzal FA, Hill AE, Arthur RM, Stover SM. 2021 Characteristics of complete tibial fractures in California racehorses. *Equine Veterinary Journal* **53**, 911–922.
63. Carrier TK, Estberg L, Stover SM, Gardner IA, Johnson BJ, Read DH, Ardans AA. 1998 Association between long periods without high-speed workouts and risk of complete humeral or pelvic fracture in thoroughbred racehorses: 54 cases (1991-1994). *Journal of the American Veterinary Medical Association* **212**, 1582–1587.
64. Wik EH, Lolli L, Chamari K, Materne O, Salvo VD, Gregson W, Bahr R. 2020 Injury patterns differ with age in male youth football: a four-season prospective study of 1111 time-loss injuries in an elite national academy. *British Journal of Sports Medicine*.
65. Armstrong DW, Rue JPH, Wilckens JH, Frassica FJ. 2004 Stress fracture injury in young military men and women. *Bone* **35**, 806–816.
66. Hughes JM, Smith MA, Henning PC, Scofield DE, Spiering BA, Staab JS, Hydren JR, Nindl BC, Matheny RW. 2014 Bone formation is suppressed with multi-stressor military training. *European Journal of Applied Physiology* **114**, 2251–2259.
67. Jacobs JM, Cameron KL, Bojescul JA. 2014 Lower extremity stress fractures in the military. *Clinics in Sports Medicine* **33**, 591–613.
68. McCalden RW, McGeough JA, Court-Brown CM. 1997 Age-related changes in the compressive strength of cancellous bone. The relative importance of changes in density and trabecular architecture. *The Journal of Bone and Joint Surgery. American Volume* **79**, 421–427.
69. Wachter NJ, Krischak GD, Mentzel M, Sarkar MR, Ebinger T, Kinzl L, Claes L, Augat P. 2002 Correlation of bone mineral density with strength and microstructural parameters of cortical bone in vitro. *Bone* **31**, 90–95.
70. Hernandez CJ, Keaveny TM. 2006 A biomechanical perspective on bone quality. *Bone* **39**, 1173–1181.
71. Chalupa RL, Aberle C, Johnson AE. 2016 Observed Rates of Lower Extremity Stress Fractures

After Implementation of the Army Physical Readiness Training Program at JBSA Fort Sam Houston. *U.S. Army Medical Department Journal* pp. 6–9.
72. Milgrom C, Finestone AS. 2017 The effect of stress fracture interventions in a single elite infantry training unit (1983-2015). *Bone* **103**, 125–130.
73. Jaworski ZF, Lok E. 1972 The rate of osteoclastic bone erosion in Haversian remodeling sites of adult dog's rib. *Calcified Tissue Research* **10**, 103–112.
74. Lassen NE, Andersen TL, Pløen GG, Søe K, Hauge EM, Harving S, Eschen GET, Delaisse JM. 2017 Coupling of Bone Resorption and Formation in Real Time: New Knowledge Gained From Human Haversian BMUs. *Journal of Bone and Mineral Research* **32**, 1395–1405.
75. Boyde A, Firth EC. 2005 Musculoskeletal responses of 2-year-old Thoroughbred horses to early training. 8. Quantitative back-scattered electron scanning electron microscopy and confocal fluorescence microscopy of the epiphysis of the third metacarpal bone. *New Zealand Veterinary Journal* **53**, 123–32.
76. McCarthy RN, Jeffcott LB. 1988 Monitoring the effects of treadmill exercise on bone by non-invasive means during a progressive fitness programme. *Equine Veterinary Journal. Supplement* **20**, 88–92.
77. Burr DB, Schaffler MB, Yang KH, Lukoschek M, Sivaneri N, Blaha JD, Radin EL. 1989a Skeletal change in response to altered strain environments: is woven bone a response to elevated strain?. *Bone* **10**, 223–233.
78. Burr DB, Schaffler MB, Yang KH, Wu DD, Lukoschek M, Kandzari D, Sivaneri N, Blaha JD, Radin EL. 1989b The effects of altered strain environments on bone tissue kinetics. *Bone* **10**, 215–221.
79. Holmes J, Mirams M, Mackie E, Whitton R. 2014 Thoroughbred horses in race training have lower levels of subchondral bone remodelling in highly loaded regions of the distal metacarpus compared to horses resting from training. *The Veterinary Journal* **202**, 443–447.
80. Whitton RC, Trope GD, Ghasem-Zadeh A, Anderson GA, Parkin TD, Mackie EJ, Seeman E. 2010 Third metacarpal condylar fatigue fractures in equine athletes occur within previously modelled subchondral bone. *Bone* **47**, 826–831.
81. Entwistle RC, Sammons SC, Bigley RF, Hazelwood SJ, Fyhrie DP, Gibeling JC, Stover SM. 2009 Material properties are related to stress fracture callus and porosity of cortical bone tissue at affected and unaffected sites. *Journal of Orthopaedic Research* **27**, 1272–1279.
82. Shan R, Johnston AS, Rosanowski SM, O'Shea J, Riggs CM. 2022 Stress fracture of the palmar, distal cortex of the third metacarpal bone: A diagnostic challenge with a good prognosis. *Equine Veterinary Journal* **54**, 74–81.
83. O'Sullivan CB, Lumsden JM. 2003 Stress fractures of the tibia and humerus in Thoroughbred racehorses: 99 cases (1992-2000). *Journal of the American Veterinary Medical Association* **222**, 491–8.
84. Piotrowski G, Sullivan M, Colahan PT. 1983 Geometric properties of equine metacarpi. *Journal of Biomechanics* **16**, 129–139.
85. Nunamaker DM, Butterweck DM, Provost MT. 1989 Some geometric properties of the third metacarpal bone: A comparison between the thoroughbred and standardbred racehorse. *Journal of Biomechanics* **22**, 129–134.
86. Davies HMS. 2006 Estimating peak strains associated with fast exercise in Thoroughbred racehorses. *Equine Veterinary Journal* **38**, 383–386.
87. Nunamaker DM, Butterweck DM, Provost MT. 1990 Fatigue fractures in thoroughbred racehorses: relationships with age, peak bone strain, and training. *Journal of Orthopaedic Research* **8**, 604–611.
88. Merritt JS, Davies HMS. 2010 Metacarpal geometry changes during Thoroughbred race training are compatible with sagittal-plane cantilever bending: Cantilever bending of the equine metacarpus. *Equine Veterinary Journal* **42**, 407–411.